Remote Sensing of Environment 131 (2013) 38–50

Contents lists available at SciVerse ScienceDirect

Remote Sensing of Environment

journal homepage: www.elsevier.com/locate/rse

Assessment of satellite-derived diffuse attenuation coefficients and euphotic depths in south Florida coastal waters

Jun Zhao [a], Brian Barnes [a], Nelson Melo [b,c], David English [a], Brian Lapointe [d], Frank Muller-Karger [a], Blake Schaeffer [e], Chuanmin Hu [a,*]

[a] College of Marine Science, University of South Florida, 140 Seventh Avenue, South, St. Petersburg, FL 33701, United States
[b] NOAA, Atlantic Oceanographic & Meterological Laboratory, United States
[c] University of Miami, Cooperative Institute for Marine and Atmospheric Studies, United States
[d] Harbor Branch Oceanographic Institute at Florida Atlantic University, United States
[e] US Environmental Protection Agency, United States

ARTICLE INFO

Article history:
Received 28 December 2011
Received in revised form 16 October 2012
Accepted 4 December 2012
Available online xxxx

Keywords:
Ocean color
Remote sensing
MODIS
SeaWiFS
Bio-optical algorithm
Diffuse attenuation coefficient
Euphotic depth

ABSTRACT

Optical data collected in coastal waters off South Florida and in the Caribbean Sea between January 2009 and December 2010 were used to evaluate products derived with three bio-optical inversion algorithms applied to MODIS/Aqua, MODIS/Terra, and SeaWiFS satellite observations. The products included the diffuse attenuation coefficient at 490 nm (K_d_490) and for the visible range (K_d_PAR), and euphotic depth (Z_{eu}, corresponding to 1% of the surface incident photosynthetically available radiation or PAR). Above-water hyperspectral reflectance data collected over optically shallow waters of the Florida Keys between June 1997 and August 2011 were used to help understand algorithm performance over optically shallow waters. The in situ data covered a variety of water types in South Florida and the Caribbean Sea, ranging from deep clear waters, turbid coastal waters, and optically shallow waters (K_d_490 range of ~0.03–1.29 m^{-1}). An algorithm based on Inherent Optical Properties (IOPs) showed the best performance (RMSD < 13% and R^2 ~1.0 for MODIS/Aqua and SeaWiFS). Two algorithms based on empirical regressions performed well for offshore clear waters, but underestimated K_d_490 and K_d_PAR in coastal waters due to high turbidity or shallow bottom contamination. Similar results were obtained when only in situ data were used to evaluate algorithm performance. The excellent agreement between satellite-derived remote sensing reflectance (R_{rs}) and in situ R_{rs} suggested that the different product uncertainties resulted primarily from algorithm inversion as opposed to atmospheric correction. A simple empirical model was developed to derive Z_{eu} from K_d_490 for satellite measurements of nearshore waters. MODIS/Aqua gave the best results in general relative to in situ observations. Our findings lay the basis for synoptic time-series studies of water quality in coastal ecosystems, yet more work is required to minimize the bottom interference in the Florida Keys optically shallow waters.

1. Introduction

The management of coastal resources requires systematic assessments of water quality. A common index of water quality is water clarity, estimated by the diffuse attenuation coefficient for downwelling irradiance (K_d). This parameter allows prediction at various depths of the availability of light to marine organisms including coral and seagrass communities (Duarte, 1991; Yentsch et al., 2002). Programs to monitor and understand water quality and ecologic health in coastal ocean areas are conducted around the world. Most, if not all, programs lack the high frequency and synoptic scope required to understand the high spatial and temporal variability that is typical of coastal environments. Since 1995 the Florida Bay Water Quality Monitoring Program (Boyer et al., 1997) and the South Florida Program and Florida Bay Program that was established in 1996 (Kelble & Boyer, 2007; Kelble et al., 2005) are examples of intensive programs designed to assess long-term spatial and temporal changes in coastal water quality. These programs provide a diverse range of measurements which allows the testing of new water quality assessment methods using satellite sensors. Satellite imagery, on the other hand, increases data collection frequency and expands the areal coverage. The combination of data from both the satellite sensors and the monitoring programs can be used to test hypotheses related to the relationship between short-scale variability and long-term water quality patterns over large areas. The field data, for example, are collected infrequently (~1–3 month intervals) at pre-defined discrete sampling locations, while the satellite imagery is collected at near daily frequencies.

Satellite sensors now routinely provide synoptic and frequent measurements of the spectral reflectance of the surface ocean, from which

* Corresponding author. Tel.: +1 727 5533987.
E-mail address: hu@marine.usf.edu (C. Hu).

0034-4257/$ – see front matter © 2012 Elsevier Inc. All rights reserved.
http://dx.doi.org/10.1016/j.rse.2012.12.009

various bio-optical products are derived. These products, however, may contain significant uncertainties for coastal waters. In this study we sought to determine the appropriate algorithms to apply to satellite observations for the estimation of water clarity and light availability in coastal waters off South Florida and the northern Caribbean Sea. An attempt is made to quantify the uncertainties of the satellite-derived products, and their applicability in establishing a long-term time series. We address only satellite products to estimate light penetration and euphotic depth such as K_d_490, K_d_PAR, and euphotic depth (Z_{eu}, defined as the depth of 1% of surface photosynthetically available radiation or PAR).

There are at least two reasons to focus this study on the K_d and related products. First, these are ecologically-important indices that allow estimation of the availability of light to underwater communities, which provide critical information for the SW Florida coastal ocean ecosystem. Second and most importantly, our knowledge on the quality of these products is poor. Indeed, although satellite-derived chlorophyll-a data products have been evaluated extensively for the global oceans and many regional coastal waters (e.g., Gregg & Casey, 2004; Hu et al., 2003a; Marrari et al., 2006; McClain, 2009; McClain et al., 2004; Zhang et al., 2006), validation of K_d products has been rare, possibly due to the technical difficulty in measuring K_d in the field, as compared with chlorophyll-a measurements. To our knowledge, only three refereed articles (Lee et al., 2005a; Mélin et al., 2007; Wang et al., 2009) compared satellite and in situ K_d using limited field data. Indeed, for the entire SeaWiFS mission (1997–2010), the NASA SeaBASS search engine (http://seabass.gsfc.nasa.gov/seabasscgi/validation_search.cgi) yielded only 465 K_d data points, with none in the Gulf of Mexico. In contrast, the same search yielded 2087 chlorophyll-a data points.

Therefore, given the need by both research community and environmental groups in the understanding of the light environment in the SW Florida coastal waters and the lack of knowledge of the validity of satellite-based K_d products, our objectives were to 1) collect high-quality K_d data from repeated cruise surveys; and 2) validate the various satellite-based products and make recommendations for product use in coastal waters.

2. Algorithms and satellite-derived products

Since the launch of the Coastal Zone Color Scanner (CZCS) onboard the Nimbus-7 satellite in 1978, significant advances have been made in the spatial and temporal coverage, spectral and radiometric resolution, and subsequently derived product quality of modern satellite ocean color instruments (Darecki & Stramski, 2004; McClain, 2009; Morel, 1998). Of particular interest are the Sea-viewing Wide Field-of-view Sensor (SeaWiFS, 1997–2010), and the Moderate Resolution Imaging Spectroradiometer (MODIS Terra, 1999–present; MODIS Aqua, 2002–present), because they provide long time series of global observations at approximately 1 km spatial resolution.

The NASA SeaDAS software package (Baith et al., 2001) offers several algorithms to derive K_d_490 and associated data products (e.g., Z_{eu}) from these satellite sensors. The "default" algorithm is based on an empirical regression between field-measurements of K_d_490 and the blue-green band ratio of normalized water-leaving radiance (nL_w) (Mueller, 2000; Mueller & Trees, 1997). Similar to the blue-green band ratio algorithm employed to estimate chorophyll-a concentrations (Chl, O'Reilly et al., 1998), the Mueller (2000) algorithm was designed for Case I waters where the variability of phytoplankton and their direct degradation products are the dominant factor controlling the optical conditions of the near-surface waters

$$K_d\_490 = 0.016 + 0.15645\left[\frac{nL_w(490)}{nL_w(555)}\right]^{-1.5401}. \quad (1)$$

Here, the labels 490 and 555 denote the center wavelengths (in nm) of particular sensor bands. The coefficients in Eq. (1) were evaluated using a global dataset (Werdell, 2005) to yield:

$$K_d\_490 = 0.1853\left[\frac{nL_w(490)}{nL_w(555)}\right]^{-1.349} \quad (2)$$

Similar region-specific algorithms have been developed to account for different types of turbid waters (Doron et al., 2007; McKee et al., 2007; Wang et al., 2009).

Another empirical algorithm implemented in SeaDAS to derive K_d_490 uses satellite-derived chlorophyll a estimates instead of the blue-green band ratio of Eq. (1) as the independent variable (Morel, 1988; Morel & Maritorena, 2001; Morel et al., 2007a):

$$K_d\_490 = 0.0166 + 0.0773[Chl]^{0.6715}. \quad (3)$$

The sole dependence of K_d_490 on chlorophyll a is characteristic of an algorithm designed for Case I waters (Morel & Prieur, 1977) where optical properties are dominated by phytoplankton and their direct degradation products, or where all optically significant constituents covary (Lee & Hu, 2006).

These algorithms work well for Case I waters, but produce large uncertainties in turbid and shallower coastal waters. Lee et al. (2005a) identified several factors producing the large uncertainties in these empirical algorithms. Specifically, empirical coefficients are most applicable to the datasets used to derive them; band ratios are not only sensitive to changes in the magnitude of nL_w, but also to the asymptotic optical properties as concentrations of optically significant constituents increase; and the effect of sun angle is not considered. Based on these considerations and radiative transfer simulations, Lee et al. (2005b) proposed a semi-analytical algorithm to estimate K_d_490, using two steps: (1) estimating the total absorption coefficient (a, m^{-1}) and total backscattering (b_b, m^{-1}) at 490 nm from spectral nL_w (i.e. using Lee et al., 2002, 2005a, 2007); (2) then deriving K_d_490 from a and b_b using:

$$K_d\_490 = (1 + 0.005\theta_0)a(490) + 4.18\left(1 - 0.52e^{-10.8a(490)}\right)b_b(490) \quad (4)$$

The solar zenith angle, θ_0, is determined above the water's surface.

While all three K_d_490 algorithms are implemented in the present version of SeaDAS, few studies have evaluated the validity of K_d_490 in either the open ocean or in coastal waters, perhaps due to the difficulty in obtaining high-quality in situ K_d_490 data. Lee et al. (2005a) evaluated the performance of the above three algorithms using data from both oceanic and coastal waters with K_d_490 ranging from ~0.04 to 4 m^{-1}. They showed that the empirical algorithms provided satisfactory results in oceanic waters with relatively low K_d_490 values, but produced significant errors in turbid coastal waters. In contrast, K_d_490 derived from Eq. (4) showed wider applicability for both oceanic and coastal waters. Mélin et al. (2007) demonstrated overestimation (underestimation) of the satellite-derived K_d_490 for low (high) K_d_490 values in the northern Adriatic Sea (K_d_490 ranged between 0.03 and 0.5 m^{-1}) using both empirical and semi-analytical algorithms (Lee et al., 2005b; Mueller, 2000; Werdell, 2005). Wang et al. (2009) showed that both Mueller and Lee models underestimated K_d_490 for turbid Chesapeake Bay waters where K_d_490 ranges from 0.4 to 5 m^{-1}. To our knowledge, Lee et al., Mélin et al. and Wang et al. are the only three published papers that compared the performance of both empirical and semi-analytical algorithms for deriving K_d_490. The validity of satellite-based K_d products is unknown for the entire Gulf of Mexico. Here we test these algorithms in coastal waters off South Florida.

3. Field data collection and processing

Seven oceanographic surveys using the R/V Walton Smith were conducted in south Florida coastal waters and the Caribbean Sea between January 2009 and December 2010 (Table 1) to assess the physical oceanographic conditions affecting regional ecosystems. Optical data were collected at selected stations using a PRR-2600 optical profiler (Biospherical Instruments Inc.) following the protocols of Mueller et al. (2003), which are briefly described below.

The PRR-2600 instrument measures downwelling irradiance (E_d, mW cm^{-2} μm^{-1}) and upwelling radiance (L_u, mW cm^{-2} μm^{-1} s r^{-1}) in 7 spectral channels centered at 380, 443, 490, 555, 589, 625, and 683 nm. It also measures or computes PAR (400 to 700 nm), solar-stimulated (or 'natural') fluorescence, sensor orientation information, water temperature, and temperature of the detector array. Ideally, PAR should be measured as scalar irradiance of the entire 4π solid angle in units of quanta (photons) instead of a vector irradiance (E_d) of the downwelling 2π solid angle in units of power (Watts). However, Morel and Gentili (2004) presented a thorough investigation on the difference between these two methods in affecting the K_d_PAR measurements, and concluded that the difference was at most 6% and often much smaller for a variety of water types. Thus, given the wide usage of this commercially available instrument (including Lee et al., 2007), such measured PAR was regarded as a valid approximation of the ideal PAR, and used to derive K_d_PAR and euphotic depth.

The instrument was deployed at 66 stations, with 54 located in South Florida coastal waters and 12 in the Caribbean Sea (Fig. 1). At each station, the instrument was lowered from the ship side that faced the sun to avoid ship shadow after being stabilized for about 10 min in the water. Usually this allows the instrument to drift further away (~10 m) to avoid potential ship-reflected light. Dark offset measurements were recorded at the beginning of each profile for 45–60. With the hand-controlled cable, the instrument was lowered in a free-falling mode at a steady downward speed of about 0.5 m s^{-1}. Both downcast and upcast data were recorded, and the cast was repeated several times for quality control, as well as to obtain a mean measurement profile. During the upcast, extra caution was used to assure that the sensor was not tilted when the cable was pulled. During post processing data with tilt angles > 10° were discarded. No above-water sensor was used to measure the downwelling irradiance, so the instrument was deployed only when the possibility that clouds would obscure the sun was slight.

After correction of the measurement profile with the appropriate dark offset, K_d was derived using a non-linear fit between downwelling irradiance (E_d) and depth (z):

$$E_d(z,\lambda) = E_d(0^-,\lambda)\exp[-K_d(\lambda)z].$$

The downwelling irradiance $E_d(0^-)$ is defined just beneath the water–air interface. Once K_d and $E_d(0^-)$ were determined from the non-linear regression, $E_d(0^+)$ was estimated using

$$E_d\left(0^+,\lambda\right) = E_d(0^-,\lambda)(1+\alpha)$$

where α is a factor accounting for the surface Fresnel reflection and light refraction across the air–sea interface, and was taken as 0.043 (Smith & Baker, 1984). This procedure was applied to all radiometric measurements.

The choice of depths used for derivation of K_d can have a significant impact on the resulting K_d value (Lee et al., 2005a). Visual examination of the E_d profile was used to chosen an upper bound (z_1) for a mathematical fit that would have minimal surface wave-focusing effects, but the choice of the lower bound (z_2) was not straightforward. Because 90% of the surface ocean color signal comes from the water column above 1 optical depth (Gordon & McCluney, 1975), the depth corresponding to 1 optical depth (OD) was chosen as the lower bound through an iterative process (Mueller et al., 2003). Examination of the extrapolated $E_d(0^+)$ provided another quality control to verify the validity of the derived K_d. The estimated $E_d(0^+)$ was compared with that estimated using the RADTRAN atmospheric radiative transfer model (Gregg & Carder, 1990). When the depth corresponding to 1 OD was chosen as the lower bound (z_2), the $E_d(0^+)$ estimate agreed with the RADTRAN estimate to within 10%. Therefore, in this study the lower bound of depth to estimate K_d was always chosen to correspond to 1 OD according to the Mueller et al. (2003) method.

Deriving remote sensing reflectance (R_{rs}) from the PRR2600 measurements requires correction of the L_u signal from instrument self-shading (Gordon & Ding, 1992; Zibordi & Ferrari, 1995), which is related to the instrument size (effective radius or R), total absorption coefficient of the water column (a), and the proportion of direct and diffuse light. The PRR2600 has an effective radius of 0.05 m. a was not measured, but was approximated from the PRR2600 measured K_d and Eq. (4). The direct and diffuse components in E_d were estimated using the RADTRAN model. Then, after the correction of the self-shading effect, L_u vertical profile was used to derive the water-leaving radiance (L_w) following Mueller et al. (2003). Finally, R_{rs} was derived as $R_{rs} = L_w/E_d(0^+)$.

All in situ data were checked for quality, and measurements considered suspicious were discarded or flagged. Quality flags included excessive instrument tilt (>10°), large differences (>10%) between measurements from the downcast and the upcast, and large differences (>10%) between the repeated profiles at the same station. This procedure flagged most of the data collected at stations along both the shallow Florida Reef Tract and shallow waters in the Caribbean as "low-quality" shown in Fig. 1a and b. Data from these stations were not used to evaluate the satellite algorithms and products in this study.

In order to illustrate bottom contamination, seventy-one in situ multispectral remote sensing reflectance (R_{rs}) measurements taken between June 1997 and August 2011 in the optically shallow waters (2.5 m<depth<20 m) south of the Florida Keys were examined (Fig. 1c). Remote sensing reflectance was measured using a custom-built spectral radiometer (Spectrix, 400 to 800 nm, ~2.5 nm resolution; Bissett et al., 1997; N = 36) or hyperspectral surface acquisition system (HyperSAS, Satlantic Inc., 350–800 nm at ~1 nm resolution; N = 35). Both instruments measured the above-water radiance ($L_t(\lambda)$),

Table 1
Location and time of the seven cruise surveys to measure ocean properties.

Region	Date	Cruise ID	# of stations	Measured data[a]
South FL coastal waters	Jan 21–25, 2009	WS0901	7	L_u, E_d, T, S, CDOM, Chl
South FL coastal waters	Aug 23–27, 2009	WS0914	14	L_u, E_d, T, S, CDOM, Chl
South FL coastal waters	Oct 26–Nov 5, 2009	WS0919	1	L_u, E_d, T, S, CDOM, Chl
South FL coastal waters	Dec 13–17, 2009	WS0923	15	L_u, E_d, T, S, CDOM, Chl
South FL coastal waters	May 3–7, 2010	WS1007	9	L_u, E_d, T, S, CDOM, Chl
South FL coastal waters	Dec 2–4, 2010	WS1022	8	L_u, E_d, T, S, CDOM, Chl
Caribbean Sea	Feb 23–Mar 14, 2010	NF1001	12	L_u, E_d, T, S, CDOM, Chl

[a] L_u denotes upwelling radiance, E_d denotes downweling irradiance, T denotes temperature, S denotes salinity, CDOM denotes colored dissolved organic matter fluorescence, and Chl denotes chlorophyll a fluorescence.

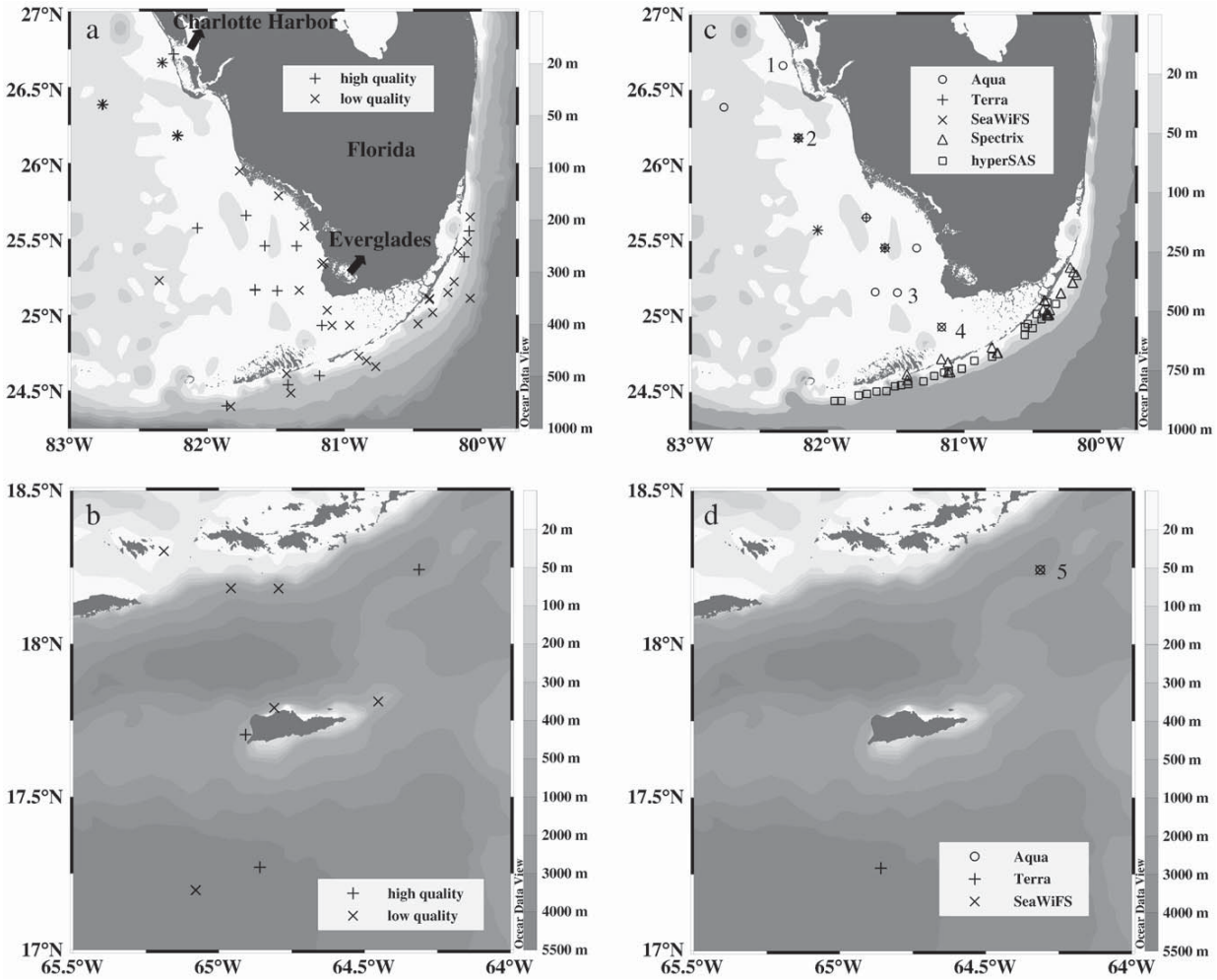

Fig. 1. Bathymetry map showing station locations where downwelling irradiance and upwelling radiance were measured using a PRR2600 optical profiler. (a) Six cruise surveys were conducted in south Florida coastal waters between January 2009 and December 2010. Stations A and B are noted in (a), where sensitivity of PRR2600-derived K_d on the depth interval was studied. (b) A single cruise survey was conducted in the Caribbean Sea between 23 February and 2 March 2010. Of the 66 stations, those with concurrent cloud-free satellite measurements (MODIS/Aqua, MODIS/Terra, and SeaWiFS) within ±44 h are annotated in (c) and (d) for the two regions, respectively. Five stations, noted as 1–5 in (c) and (d) were used to show the spectral K_d. The open triangles and squares in (c) indicate stations where R_{rs} measurements in optically shallow waters were collected using custom-built (Spectrix) and HyperSAS spectrometers between June 1997 and August 2011 (N = 71). A rigorous quality control procedure (see text) determined a "high" or "low" data quality flag, with the former used in the satellite data product assessment.

sky radiance ($L_i(\lambda)$), and downwelling sky irradiance ($E_s(\lambda)$), from which (R_{rs}) was derived (Lee et al., 1997; Mobley, 1999). Note that no K_d profiling measurement was conducted from these optically shallow waters.

4. Satellite data processing

Level-1 data from MODIS/Aqua, MODIS/Terra, and SeaWiFS corresponding to the cruise periods were obtained from the U.S. NASA Goddard Space Flight Center and processed using SeaDAS (version 6.1) default algorithm settings. Three K_d_490 products were generated using the Mueller algorithm (Werdell, 2005, Mueller algorithm, K_d_490_mueller), the Morel et al. (2007a) algorithm (Morel algorithm, K_d_490_morel), and the Lee et al. (2005b) algorithm (Lee algorithm, K_d_490_lee). Two K_d_PAR estimates were also generated. The first was derived using an empirical algorithm (Morel et al., 2007a K_d_PAR_morel), and the second using a semi-analytical IOP-based algorithm (Lee et al., 2007, K_d_PAR_lee). SeaDAS produces both of these estimates, as well as a corresponding estimate of Z_{eu}, i.e. Z_{eu}_morel and Z_{eu}_lee. R_{rs} at 412 nm, 443 nm, 488 (490 for SeaWiFS), 547 nm (555 nm for SeaWiFS), and 667 nm (670 nm for SeaWiFS) were also generated.

5. Method for satellite — in situ comparison

All satellite data with poor quality, as defined by the quality-control flags in the data products (i.e., problems due to clouds, stray light, atmospheric correction failure, high top-of-atmosphere radiance, low water-leaving radiance, large solar/viewing angles, and navigation failure), were discarded. Second, the acceptable time interval within which the satellite and in situ measurements were considered as "concurrent" was adjusted from community-accepted threshold (<±3 h, Bailey & Werdell, 2006). We first tried the <±3 h time window, but found this criterion excluded many high-quality in situ data due to frequent cloud cover in the satellite measurements. Specifically, this criterion produced 9 in situ and satellite data matching pairs for MODIS-Aqua, 3 pairs for MODIS-Terra, and 3 pairs for SeaWiFS. In order to maximize the number of possible matching

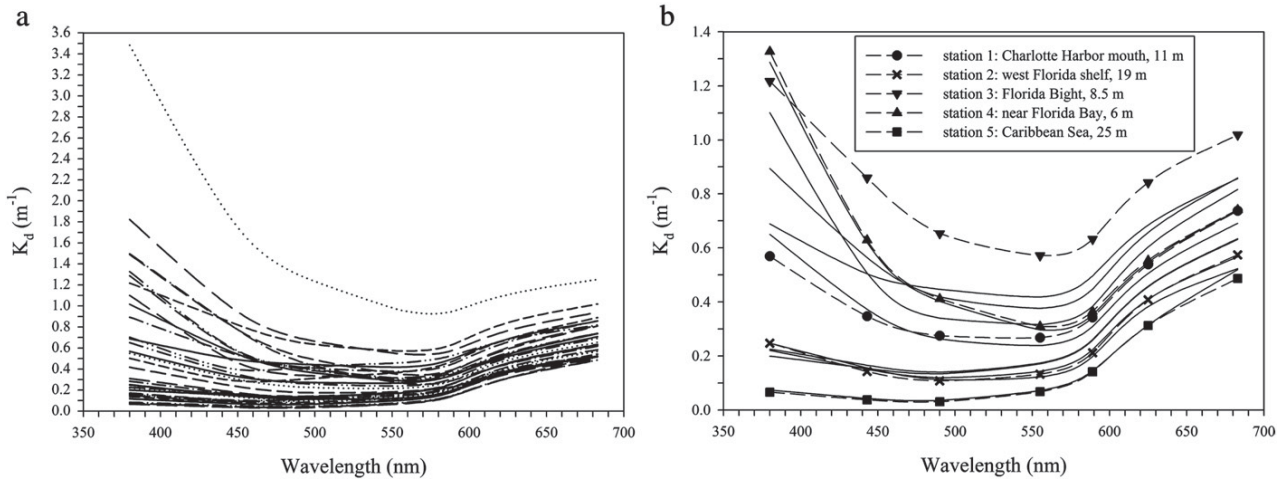

Fig. 2. (a) $K_d(\lambda)$ derived from the PRR2600 measurements for 34 stations determined as "high quality" as shown in Fig. 1. (b) $K_d(\lambda)$ derived from the PRR2600 measurements for all 15 stations with matched satellite data, and 5 of them (Fig. 1c and d) are selected to represent typical spectral shapes and magnitudes from all stations. Note that these data covered nearly all water types in the study region.

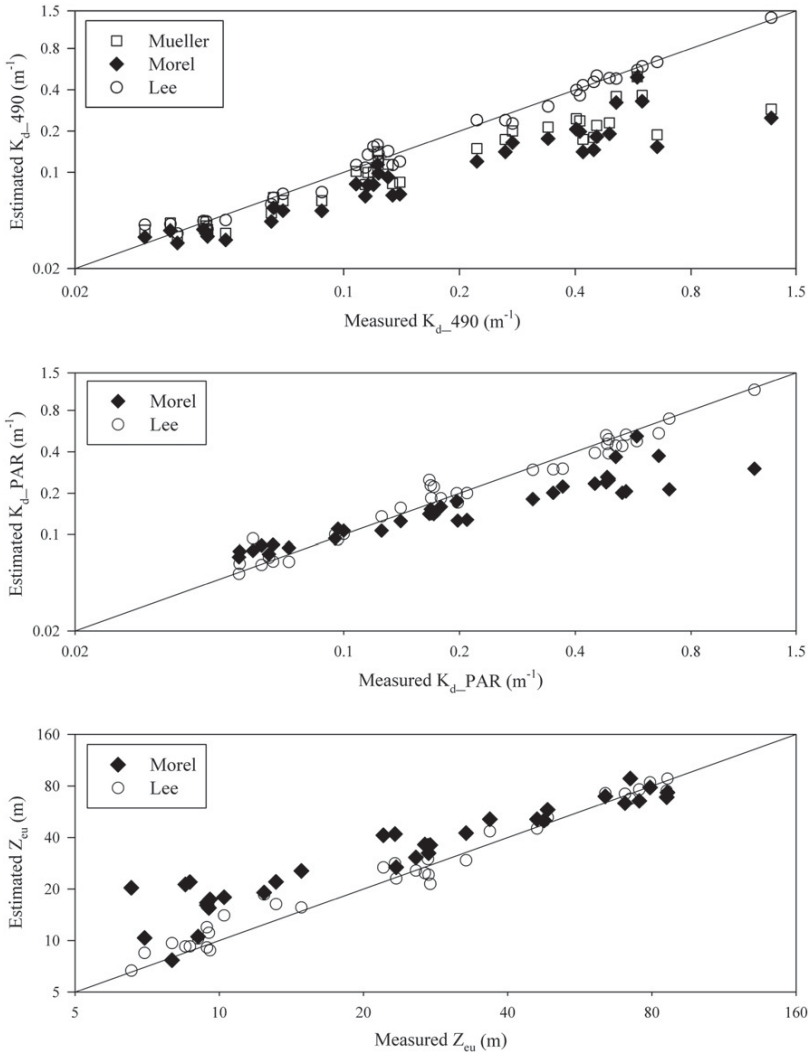

Fig. 3. Comparison between PRR2600-measured parameters (K_d_490, K_d_PAR, and Z_{eu}) and those estimated from in situ R_{rs} data using three inversion algorithms. The solid lines are the 1:1 lines.

Table 2
Uncertainties in the algorithm derived K_d_490 (m^{-1}), K_d_PAR (m^{-1}) and Z_{eu} (m) when in situ R_{rs} data from the PRR2600 measurements were used as the algorithm inputs. RPD: Relative Percentage Difference. RMSD: Root-Mean-Square Difference (in percent).

Parameter	N	Range	Mean	Algorithm	Mean ratio	RPD (%)	RMSD (%)	Slope	Intercept	R^2
K_d_490	34	0.03–1.29	0.26 ± 0.26	Mueller	0.75	−25.05	34.67	0.32	0.06	0.61
				Morel	0.64	−36.29	42.08	0.29	0.05	0.56
				Lee	1.01	0.95	13.11	1.01	0.00	0.99
K_d_PAR	34	0.054–1.17	0.30 ± 0.25	Morel	0.81	−19.47	37.07	0.31	0.08	0.61
				Lee	1.02	1.64	18.26	0.90	0.02	0.97
Z_{eu}	34	6.56–86.24	31.10 ± 25.98	Morel	1.50	50.35	77.39	0.82	11.58	0.91
				Lee	1.07	7.32	16.36	0.98	1.60	0.98

pairs between in situ and satellite observations without compromising quality, the acceptable time interval was then relaxed to a longer period, which was determined through trial and error as 44 h. With this new criterion, 4 more matching data pairs for MODIS-Aqua, 2 more for MODIS-Terra, and 4 more for SeaWiFS were found. The quality of these additional satellite data (>±3 h but <±44 h), in terms of temporal variability was determined through a temporal variance check by comparing them to satellite data obtained from ±120 h of the in situ measurements. The variance was defined as the standard deviation divided by the mean from all satellite data within the ±120 h time window. For the additional satellite data, temporal variance within the ±120 h time window ranged from 2% to 16.7%, with a mean of 11.4% (±5%). This is actually comparable to the uncertainties in the in situ K_d_490. Thus, data from the extended ±44 h time window were used for the satellite-in situ comparison.

A satellite image pixel covered at least 1 km^2 and sub-pixel spatial variability could produce large differences when individual in situ measurements are compared to satellite derived estimates (Hu et al., 2004a). Therefore, a spatial homogeneity test was applied to the satellite data. The following criteria were used in this test (Bailey & Werdell, 2006): (1) half of the pixels in the 3×3 window centered around the in situ station must have valid data, and the variance from these valid pixels must be <10%; (2) spatial variations in temperature, salinity, CDOM fluorescence, and chlorophyll-a fluorescence measurements from underway in situ sampling within an area determined by a 3×3 pixel satellite coverage are small (~<10%).

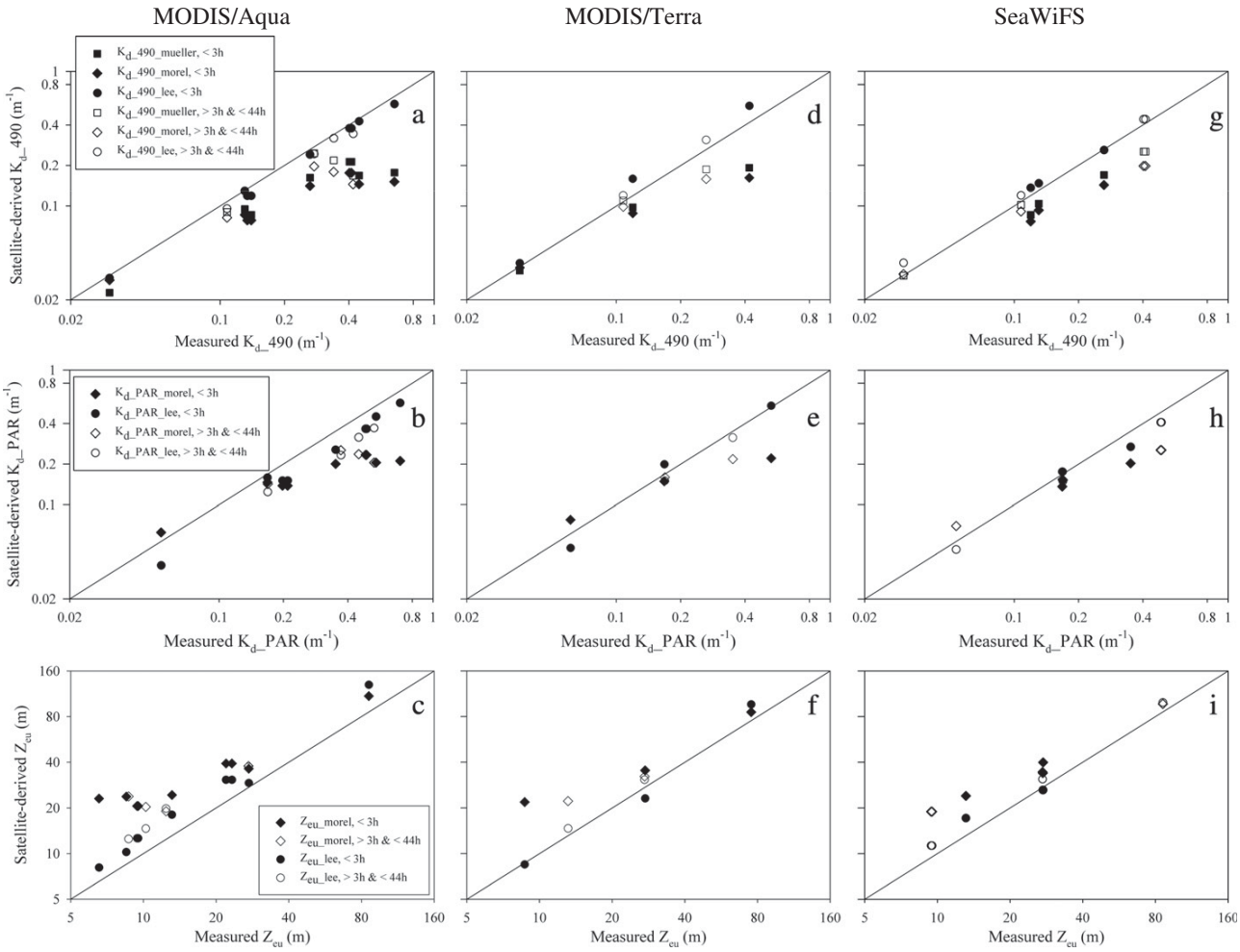

Fig. 4. Comparison between satellite-derived and PRR2600-measured K_d_490, K_d_PAR, and Z_{eu}. Solid symbols represent satellite and in situ measurements within ±3 h, and open symbols show more relaxed comparison criteria (>3 h but <44 h). Left panels: MODIS/Aqua; middle panels: MODIS/Terra; right panels: SeaWiFS.

Table 3
Uncertainties of satellite-based K_d_490 (m^{-1}) from three algorithms, as gauged by the in situ PRR2600 measurements.

Sensor	N	Range	Mean	Algorithm	Mean ratio	RPD (%)	RMSD (%)	Slope	Intercept	R^2
Aqua	13	0.03–0.65	0.29 ± 0.18	Mueller	0.60	−39.89	43.52	0.28	0.070	0.52
				Morel	0.54	−45.95	49.52	0.22	0.065	0.56
				Lee	0.91	−9.08	10.12	0.89	0.0037	0.99
Terra	5	0.035–0.42	0.19 ± 0.15	Mueller	0.79	−21.21	28.75	0.40	0.048	0.84
				Morel	0.73	−27.44	34.90	0.32	0.049	0.83
				Lee	1.20	20.24	23.03	1.33	−0.015	0.99
SeaWiFS	7	0.03–0.41	0.21 ± 0.15	Mueller	0.76	−23.66	27.63	0.56	0.024	0.99
				Morel	0.68	−32.37	37.26	0.41	0.032	0.98
				Lee	1.11	10.98	13.00	1.06	0.0045	0.995

Application of these quality control criteria resulted in the selection of 13 in situ and satellite data pairs for MODIS-Aqua, 5 pairs for MODIS-Terra, and 7 pairs for SeaWiFS as noted in Fig. 1c and d and in Table 3. These are all shallow-water stations, with bottom depths ranging between 6 m and 30 m. Several statistical measures were used to assess the differences between the satellite and in situ measurements, including mean ratios, mean percentage difference (MPD), RMS difference (RMSD), slope/intercept coefficients, as well as the coefficient of determination (R^2) between the two datasets when a linear regression was applied.

6. Algorithm evaluation: results

6.1. Statistics for K_d_490, K_d_PAR and Z_{eu}

Fig. 2a shows the PRR2600-derived spectral K_d (surface to 1 OD) for all 34 stations shown in Fig. 1, and Fig. 2b shows the spectral K_d for all 15 stations where concurrent satellite data were found for the satellite-*in situ* comparisons. The K_d spectra show substantial variability in both the spectral shape and the magnitude covering > 1 order of dynamic range in all blue-green wavelengths. K_d_490 ranged from 0.03 to 1.29 m^{-1} (40×), representing the clearest water to extremely turbid water in the study region. For clarity, K_d spectra from 5 stations with representative but contrasting spectral shapes and magnitudes are discussed here. Station 1 was located near Charlotte Harbor, where optical properties were influenced by CDOM-rich estuarine runoff (Hu et al., 2004b). A significant decrease in K_d, especially in the blue-green wavelengths, is observed to the South at Station 2. Further south, Station 3 in the Florida Bight had higher K_d values at all wavelengths, suggesting the presence of a significant amount of absorbing and scattering materials. At the time of this station's observations, the wind speed that was measured at a nearby NDBC station was about 10 m s^{-1}, enough for sediment resuspension. Station 4, in Western Florida Bay, showed K_d magnitudes similar to Station 1 for wavelengths ≥ 589 nm, but the K_d_380 was much greater, indicating that the optical environment of this station was dominated by CDOM absorption. Both Stations 3 and 4 were located in close proximity of the Florida Everglades, one of the largest wetlands in the world, with an important discharge of CDOM-rich waters. Station 5 was located in the Caribbean Sea, and provided the clearest waters used in this study. K_d values at Station 5 were similar to those arising from pure water measurements, and produced a spectral shape typical for oligotrophic Case I waters (Morel et al., 2007b).

6.2. Algorithm evaluation using in situ data only

Fig. 3 shows the performance of the three algorithms (Mueller, Morel and Lee) when in situ R_{rs} data (collected from the PRR2600 measurements) were used as the algorithm inputs, with statistical results listed in Table 2. Both Mueller and Morel algorithms worked well for K_d_490 < 0.2 m^{-1}, an upper limit for empirical algorithms (Lee et al., 2005a). For higher values, both Mueller and Morel algorithms underestimated K_d_490. In contrast, the Lee algorithm showed much improved performance, with the mean ratio of 1.01 and R^2 of 0.99 between the algorithm-derived and in situ measured K_d_490. RPD and RMSD reduced to 0.95% and 13.11%, respectively. Similar improvements were found with the Lee algorithm for K_d_PAR from 0.054 m^{-1} to 1.17 m^{-1} and Z_{eu} from 6.6 m to 86.2 m.

6.3. Algorithm evaluation using satellite data

Fig. 4 shows the satellite — in situ comparisons of K_d_490, K_d_PAR and Z_{eu} with satellite data derived from MODIS/Aqua, MODIS/Terra, and SeaWiFS, respectively. The corresponding statistical results are provided in Tables 3–5.

For all three satellite instruments, when satellite-derived R_{rs} data were used in the algorithm inversion, the Mueller and Morel algorithms showed satisfactory performance for K_d_490 < 0.2 m^{-1}. For K_d_490 > 0.2 m^{-1}, both algorithms underestimated K_d_490. These results are consistent with those obtained in Section 6.2 when only in situ R_{rs} data were used in the inversions. For the entire data range, MPD ranged from −21.21% to −45.95% and RMSD was 27.63% to 49.52%. These observations are consistent with those reported in Darecki and Stramski (2004) and Lee et al. (2005a).

In contrast, K_d_490 from the Lee algorithm produced estimates with the closest agreement with the in situ values. Data scatter was reduced, with MPD and RMSD reduced to <±20% and <23%, respectively. If MODIS Terra was excluded (see below), MPD and RMSD were further reduced to ±11% and 13%, respectively. Linear regressions between MODIS/Aqua and SeaWiFS-derived K_d_490 and in situ K_d_490 had slopes close to 1 and small intercepts, with R^2 approaching 1.0. The Lee algorithm provided the best agreement between the MODIS/Aqua estimates and the in situ observations.

Similar results were observed for K_d_PAR estimates. The Morel algorithm generally performed well in clear waters (K_d_PAR < 0.2 m^{-1}), but the divergence from in situ observations increased with increasing K_d_PAR. The Lee algorithm yielded the best performance in terms of

Table 4
Uncertainties of satellite-based K_d_PAR (m^{-1}) products from two algorithms, as gauged by the in situ PRR2600 measurements.

Sensor	N	Range	Mean (m^{-1})	Algorithm	Mean ratio	RPD (%)	RMSD (%)	Slope	Intercept	R^2
Aqua	13	0.054–0.7	0.36 ± 0.19	Morel	0.62	−38.12	44.48	0.23	0.10	0.64
				Lee	0.75	−25.25	26.37	0.78	−0.010	0.97
Terra	5	0.061–0.53	0.26 ± 0.19	Morel	0.83	−17.17	33.78	0.29	0.092	0.81
				Lee	0.96	−4.38	14.54	1.01	−0.0080	0.98
SeaWiFS	7	0.054–0.49	0.27 ± 0.17	Morel	0.79	−20.71	33.31	0.38	0.072	0.96
				Lee	0.90	−10.18	14.16	0.78	0.023	0.98

Table 5
Uncertainties of satellite-based Z_{eu} (m) from two algorithms, as gauged by the in situ PRR2600 measurements.

Sensor	N	Range	Mean	Algorithm	Mean ratio	RPD (%)	RMSD (%)	Slope	Intercept	R^2
Aqua	13	6.56–85.91	20.33 ± 21.07	Morel	2.02	101.54	119.93	1.13	10.68	0.98
				Lee	1.35	35.08	37.41	1.51	−2.49	0.99
Terra	5	8.69–75.32	30.37 ± 26.48	Morel	1.56	56.22	76.30	0.99	9.28	0.99
				Lee	1.067	6.70	16.20	1.33	−5.72	0.98
SeaWiFS	7	9.42–85.91	28.59 ± 26.65	Morel	1.56	55.91	65.82	1.02	9.10	0.99
				Lee	1.13	12.62	17.28	1.14	−0.97	0.99

mean ratio, MPD, RMSD, and linear regression slope/intercept and R^2. The Lee algorithm, with its default parameterization, performed better with the data from MODIS/Terra than from the other two satellites (mean ratio of 0.96 versus 0.75 and 0.90). This was a surprise as it was well known that Terra suffered from significant striping noise due to inconsistent calibrations from the 10 detectors (Kwiatkowska et al., 2008). We believe that this was due to coincidence, as no matching pair was extracted from the low-quality (e.g., striping noise) data through the quality control process. Note that in time series analysis or data composites (weekly or monthly) such a quality control (i.e., spatial and temporal homogeneity tests) is not applied. Thus, even though the performance of Terra appears acceptable here, its use for time-series analysis is still not recommended.

Because Z_{eu} is derived using K_d_PAR, the same observations apply to Z_{eu} estimates. Specifically, with Z_{eu} ranging between 6.5 and 86 m, the Lee algorithm yielded a closer prediction to in situ measurements than the Morel algorithm, which resulted in a MPD and RMSD up to 101.54% and 119.93%, respectively.

6.4. Causes of the algorithm/product uncertainties

There are two potential reasons for a mismatch between in situ measured K_d and satellite-derived K_d. The first is the possible uncertainties in the satellite-derived spectral $R_{rs}(\lambda)$ data, which are used as the inputs of the three K_d algorithms. The second is the K_d algorithm design and applicability as well as the algorithm parameterization.

The PRR2600-derived $R_{rs}(\lambda)$, after correction of the self-shading effect, was compared with concurrent satellite-derived $R_{rs}(\lambda)$. Results showed excellent agreement between the two for all bands and all three sensors. Fig. 5 shows the comparison for two blue bands (443 and 490 nm) and one green band (555 nm). For over one order of magnitude, the uncertainties in the satellite-derived $R_{rs}(\lambda)$ are comparable to those obtained from the global open ocean waters (McClain, 2009; McClain et al., 2004). These results are also consistent from a recent validation of SeaWiFS-derived $nL_w(\lambda)$ (equivalent to $R_{rs}(\lambda)$) using historical EcoHAB data collected from adjacent coastal waters (bottom depths ranged between 10 and 100 nm) (Cannizzaro et al., submitted for publication). The agreement between satellite-derived R_{rs} and in situ R_{rs} explains why each of the three algorithms showed comparable performance regardless of the R_{rs} data source (satellite or in situ).

Thus, the mismatch between in situ measured K_d and satellite-derived K_d is not a problem of satellite-derived R_{rs}, but primarily due to the R_{rs} based K_d inversion algorithms inversion algorithms.

The Mueller and Morel algorithms were designed for phytoplankton-dominated waters, and thus yielded poor results in turbid South Florida coastal waters where the optical environment can be significantly affected by CDOM, suspended sediments, and shallow water depths. A specific data evaluation was undertaken to understand how these environmental conditions increase uncertainty in the predictions from the three algorithms.

Differences between satellite estimates and in situ measurements were plotted against $R_{rs}(670)$, which represents a proxy for water turbidity (Fig. 6). The Mueller and Morel algorithms performance degraded significantly with increasing $R_{rs}(670)$, though such a trend was not observed for the Lee algorithm's performance. This arises because the band-ratio based Mueller and Morel algorithms are sensitive to changes only in water absorption (Stramska et al., 2003), while the Lee algorithm considers both absorption and backscattering (Eq. 4).

A sensitivity test was also performed to determine potential impact of the shallow-water bottom albedo on the K_d retrievals (Maritorena et al., 1994). Following Cannizzaro and Carder (2006), a spectral curvature of $R_{rs}(412) * R_{rs}(670) / R_{rs}(555)^2$ was used to represent the relative contribution of the bottom to the R_{rs}, with a low curvature value indicating relatively higher bottom contribution. However, the data were too scattered to draw statistically meaningful conclusions. Thus, model simulations were used to assess the potential bottom effects on K_d retrievals (see discussion below).

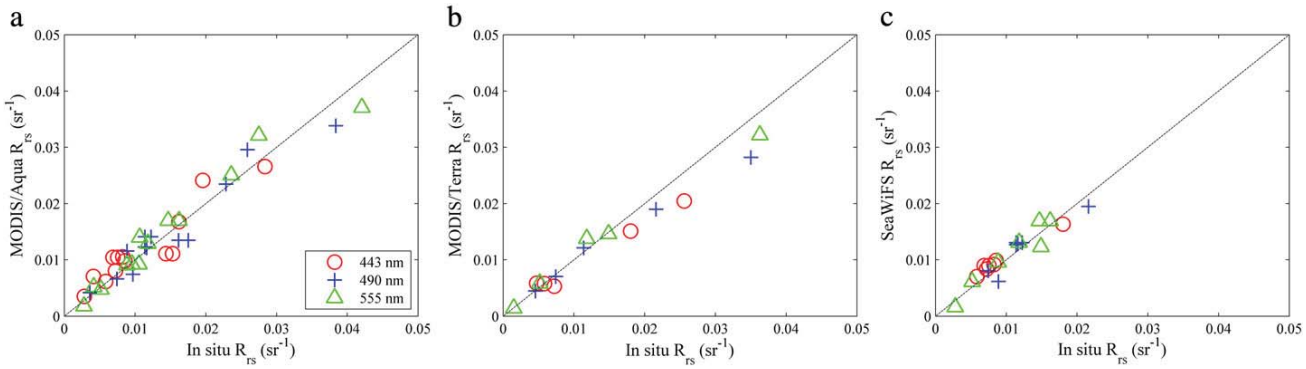

Fig. 5. Comparison between satellite-derived and in situ measured R_{rs} at 443 nm, 490 nm, and 555 nm. (a) MODIS/Aqua; (b) MODIS-Terra; (c) SeaWiFS. The in situ R_{rs} was derived from the PRR2600 measurements after correction of the instrument self-shading effect using the Gordon and Ding (1992) approach. Note that MODIS wavelengths are 443, 488, and 547 nm. Mean ratios ranged between 0.93 and 1.03, and RMS differences ranged between 11.0% and 20.0% with $R^2 > 0.9$ for all but one case. (For interpretation of the references to color in this figure legend, the reader is referred to the web version of this article.)

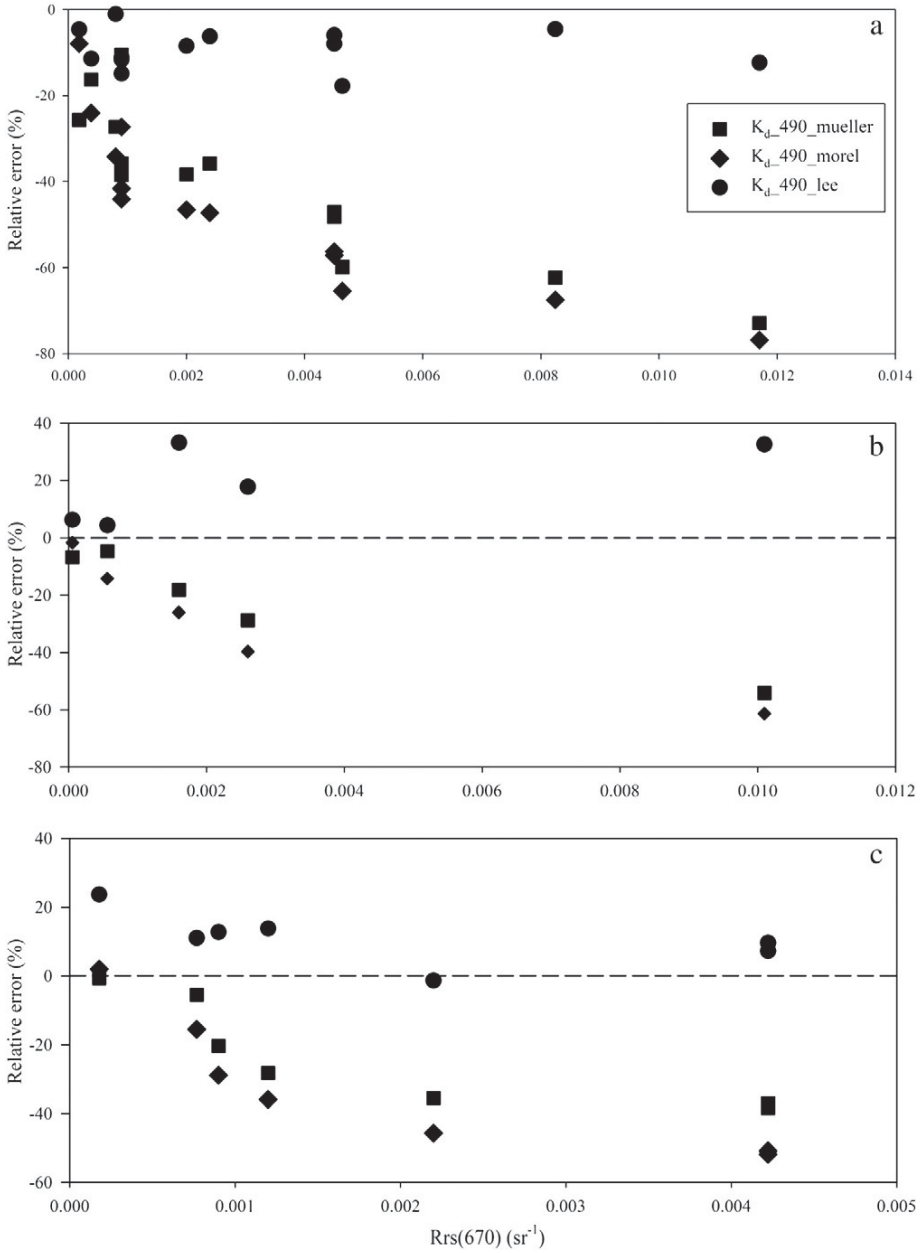

Fig. 6. Sensitivity of the K_d_490 algorithm performance to water turbidity (using $R_{rs}(670)$ as a proxy) for Aqua (a), Terra (b) and SeaWiFS (c). The PRR2600-measured K_d_490 was used to estimate the relative errors. The dashed lines show relative errors equal to 0%.

6.5. An improved Z_{eu} algorithm

All three algorithms were initially developed using global datasets. Local tuning of the coefficients can often result in better performance for regional studies. The excellent performance of the Lee algorithm in deriving K_d_490 suggests that it can be used without local tuning. However, K_d_PAR_lee and Z_{eu}_lee showed larger errors relative to in situ values, suggesting local tuning to improve performance. Fig. 7a shows a hyperbolic function used to predict Z_{eu} from the measured K_d_490. When this relationship was used with the satellite-derived K_d_490_lee to estimate Z_{eu}, a smaller difference was found between measured and satellite-derived Z_{eu} for all three instruments (Fig. 7b, Table 6). Because of the direct relationship between Z_{eu} and K_d_PAR, an improved K_d_PAR product could also be derived as $K_d\_PAR = 4.605/Z_{eu}$.

7. Discussion: product uncertainty and applicability

Several validation studies of satellite derived K_d for a variety of coastal waters have been published since the Lee et al. (2005b) algorithm became available. Lee et al. (2005a) showed that the semi-analytical method performed much better than the empirical methods in deriving K_d_490 in coastal waters. Mélin et al. (2007) showed that the Lee et al. algorithm provided a slight improvement of K_d_490 estimates when compared to the empirical band-ratio algorithms. Wang et al. (2009) found that the Lee at al. algorithm underestimated K_d_490 for turbid Chesapeake Bay waters where K_d_490 ranged between 0.4 and 5 m^{-1}. Schaeffer et al. (2011) examined the K_d_490 derived from the Lee et al. algorithm for the more turbid Louisiana shelf where K_d_490 changed from 0.08 to 6.0 m^{-1}. However,

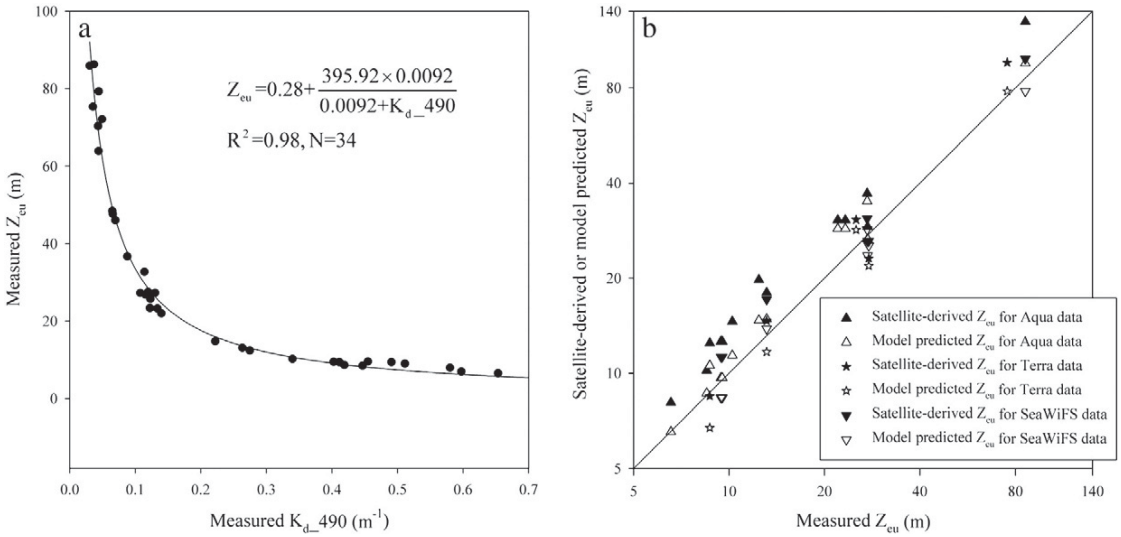

Fig. 7. (a) Relationship between measured K_d_490 and Z_{eu} (derived from in situ K_d_PAR). The solid line represents the best fit. (b) Comparison between PRR2600-measured Z_{eu} and satellite-derived Z_{eu}, where the latter was derived using the Lee et al. algorithm (solid symbols) and using the K_d_490_Lee product together with the empirical algorithm in (a) (empty symbols). The solid line depicts the 1:1 relationship.

that study used in situ K_d_PAR instead of K_d_490, while the study presented here uses in situ spectral light attenuation measurements.

The data quality thresholds used in both in situ and satellite data processing, including the strict requirements on spatial homogeneity and measurement concurrency, allowed only 15 of the 66 in situ optical profiles to be used in the algorithm/data product assessment. Thus, although the profiles contain multi-spectral information from diverse environmental conditions (Fig. 2), questions about global applicability remain. Notably, will an extrapolation of these results improve mechanisms for monitoring K_d and Z_{eu}, and thus aid longer term investigations of the causes of water clarity variability?

Two approaches were used to evaluate the applicability of these results. First, satellite estimates of K_d_490 distributions were derived with all three algorithms with MODIS/Aqua data during two seasons (May and December 2010). During the month of May, when rainfall and the wind speed was low, most offshore waters were clear with low K_d_490 values where all three algorithms produced similar results. In nearshore waters where K_d_490 was often >0.2 m^{-1}, the Lee et al. (2005a) algorithm yielded more accurate K_d_490 values. In December, episodic wind storms induced sediment resuspension in most nearshore waters where the band-ratio algorithms underestimated K_d_490 when it was >0.2 m^{-1}. These results suggest that for nearshore waters in the SW Florida the two empirical algorithms are simply not applicable.

The other approach used to examine the applicability of Lee algorithm was to perform statistical analysis of the MODIS/Aqua and SeaWiFS K_d_490_lee data products for various seasons (Terra was excluded from this analysis due to the striping noise). Fig. 8 shows the percentage of K_d_490_lee within the validation range (0.03–0.65 m^{-1}) from the 2002–2010 MODIS/Aqua measurements for the four seasons. For most of the shallow shelf waters and Florida Keys waters, the percentage of K_d_490_lee values between 0.03 and 0.65 m^{-1} is >95% for all four seasons. A smaller percentage of values in this range occurred in the clearer offshore waters, and in the inner Florida Bay and waters near the Everglades rivers (Fig. 1) where K_d_490_lee was often >0.65 m^{-1}. These rivers showed more influence on the nearshore waters during summer and autumn than during the relatively dry winter and spring months, as expected (Fig. 8).

The "applicability" results need to be interpreted carefully. The relatively low percentage during spring and summer in the offshore Florida Straits does not mean that satellite-based K_d_490_lee is not applicable for 40–60% of the time because this product has been validated elsewhere in very clear waters (K_d_490 <0.03 m^{-1}), which means general applicability in the offshore Florida Straits even if there was no direct validation from these extremely clear waters. Likewise, in nearshore turbid waters where K_d_490_lee is >0.65 m^{-1}, the product may also be valid because 1) it has been validated elsewhere (Lee et al., 2005a) for very turbid waters and 2) in situ algorithm validation in Section 6.2 showed applicability to at least 1.29 m^{-1}. On the other hand, the high percentage along the shallow Florida reef tract does not necessarily indicate that K_d_490_lee is valid for most of the time because of lack of high-quality in situ K_d measurements to compare with concurrent high-quality satellite measurements for these clear and optically shallow waters. The following model simulations were used to understand how bottom reflectance could affect K_d retrievals in these optically shallow waters.

Seventy-one in situ R_{rs} measurements taken between June 1997 and August 2011 within optically shallow waters (less than 20 m depth) of the Florida Keys (Atlantic Ocean side, Fig. 1c) were examined to understand the bottom effect. Note that during these surveys K_d was not measured, so the bottom effect was assessed through a spectra-matching optimization method (Lee et al., 1999) to explicitly remove the bottom contribution to R_{rs}. The bottom-embedded R_{rs} (i.e., the measured R_{rs}) and bottom-removed R_{rs} were both fed to the same Lee et al. (2005b) K_d algorithm, and such-derived K_d were compared with each other. Fig. 9 shows a positive relationship between K_d_490_lee derived from both R_{rs} ($R^2=0.50$, $N=62$, Slope = 1.04, Intercept = 0.09). However, a significant amount of scatter was evident, indicating large errors when the bottom-embedded K_d were used to represent the bottom-removed K_d, especially for waters with bottom depth between 5 and 10 m. When data were separated into three depth ranges, much stronger correlations were obtained.

Table 6
Uncertainties of satellite-based Z_{eu} (m) from a new empirical model (Fig. 9) and satellite-based K_d_490_lee, as gauged by the in situ PRR2600 measurements. Number of matchup pairs and data ranges are the same as in Table 4.

Sensor	Algorithm	Mean ratio	RPD (%)	RMSD (%)	Slope	Intercept	R^2
Aqua	Lee	1.12	12.40	16.51	1.12	0.35	0.99
Terra	Lee	0.93	−7.46	15.74	1.07	−2.62	0.99
SeaWiFS	Lee	0.94	−6.32	9.69	0.90	0.75	0.995

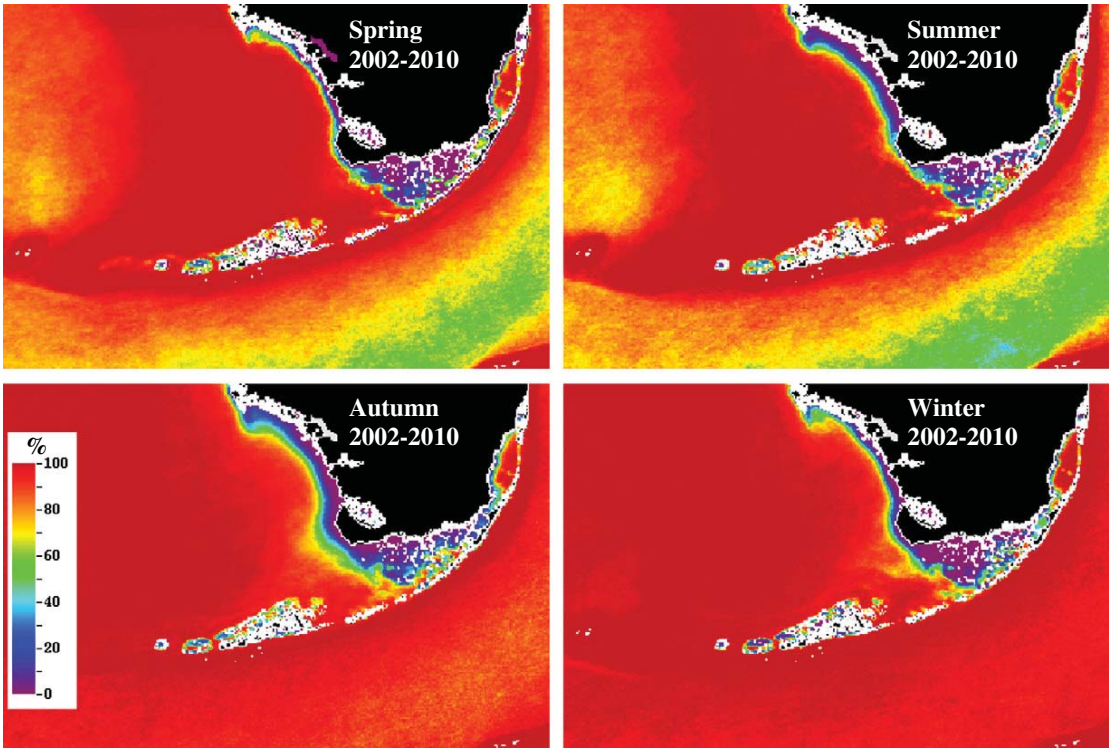

Fig. 8. Percentage of K_d_490_lee in the range of 0.03–0.65 m^{-1} from all valid (i.e., data associated with flags were discarded) MODIS/Aqua measurements for the four seasons between 2002 and 2010.

Specifically, for waters with bottom depth<5 m, a significant correlation was found between the two K_d_490_lee datasets ($R^2 = 0.83$, N = 13, Slope = 0.84, Intercept = 0.13, F = 55.28, $p < 0.0001$). Similar results were found for waters with bottom depth>10 m ($R^2 = 0.65$, N = 17, Slope = 0.98, Intercept = 0.03, F = 27.94, $p < 0.0001$). There was no significant correlation for the water depth range 5–10 m. Results for other wavelengths were similar.

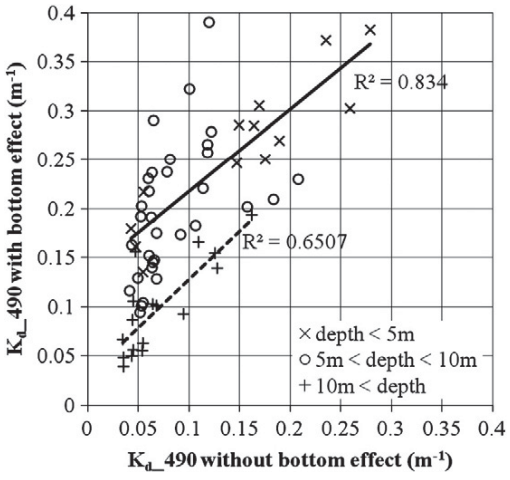

Fig. 9. Comparison between K_d_490 with bottom effect embedded and removed using the Lee et al. (1999, 2002, 2005b) algorithms and in situ R_{rs} data. Data have been separated according to bottom depths at measurement stations: $2 < z \leq 5$ m $5 < z \leq 10$ m and $10 < \text{depth} \leq 20$ m. Linear regression lines and R^2 are shown for the first and last depth ranges.

The spectra-matching algorithm to remove the bottom effect has been validated for hyperspectral data (Lee et al., 1999), but has shown variable performance over multi-band satellite data (Hu et al., 2003b). Fig. 9 suggests that depth-specific K_d regression may be used to scale the satellite-derived K_d_490_lee to more realistic values in the absence of explicit removal of the bottom-perturbed satellite-derived K_d_490 retrievals for bottom depths<5 m and >10 m. For intermediate depth ranges (between 5 and 10 m) around the Florida Keys Reef Tract (Fig. 1c), the uncertainties of satellite-based K_d_490_lee are too large for use in a reliable time-series analysis. The amount of in situ observations presently available for the optically shallow waters in the Florida Keys, particularly along the Florida Reef Tract, is insufficient for rigorous validation and adjustment of satellite algorithms.

8. Conclusion

Although the empirical band-ratio algorithms provide satisfactory estimates of K_d_490 and Z_{eu} in oligotrophic waters, the estimates diverge from in situ measurements made in South Florida coastal waters. In contrast, the IOP-based algorithm produces satisfactory K_d_490 and Z_{eu} estimates for a variety of water types, including the South Florida coastal waters. Thus, though the empirical band-ratio algorithms are commonly used in satellite data processing, e.g. SeaDAS, the K_d_490 and Z_{eu} estimates from the Lee algorithm should provide a more accurate estimate for long-term water clarity studies and efforts to assess ecosystem response to episodic events in coastal waters. Statistics from in situ validation and satellite data analysis suggest the estimates from the IOP-based algorithm have sufficient fidelity to allow their use for temporal analysis of the South Florida coastal waters.

Present validation efforts are hindered by the paucity of concurrent high-quality in situ and satellite K_d measurements over most of the optically shallow waters in the Florida Keys and Florida Bay. While a provisional approach would be to model the influence of

various bottom albedos on R_{rs} for a variety of bottom depths, a preferable approach would be to collect high-quality in situ data in these waters and improve the algorithms that reduce the perturbation of R_{rs} in optically shallow waters.

Acknowledgments

This study was supported by the U.S. NASA Biology and Biogeochemistry Program, Gulf of Mexico Program, and Water and Energy Cycle Program. Field support came from the South Florida Program (SFP) of NOAA's Atlantic Oceanographic and Meteorological Laboratory. The SFP has been funded by the NOAA/OAR Ship Charter Fund, NOAA's Center for Sponsored Coastal Ocean Research, NOAA's Deepwater Horizon Supplemental Appropriation, and the US Army Corps of Engineers. We are indebted to the NASA Ocean Biology Processing Group (OBPG) who distributed the SeaDAS software package as well as MODIS and SeaWiFS data. We also want to thank George Craven, John Lehrter, and Jessica Aukamp from the US EPA, as well as the crew of the R/V F. G. Walton Smith for their assistance in collecting the in situ data. We are thankful to two anonymous reviewers who provided substantial comments and suggestions that led to the improvement of this manuscript.

References

Bailey, S. W., & Werdell, P. J. (2006). A multi-sensor approach for the on-orbit validation of ocean color satellite data products. *Remote Sensing of Environment*, *102*, 12–23.

Baith, K., Lindsay, R., Fu, G., & McCain, C. R. (2001). Data analysis system developed for ocean color satellite sensors. *EOS*, *82*, 202.

Bissett, W. P., Patch, J. S., Carder, K. L., & Lee, Z. P. (1997). Pigment packaging and Chl a specific absorption in high-light oceanic waters. *Limnology and Oceanography*, *42*, 962–968.

Boyer, J. N., Fourqurean, J. W., & Jones, R. D. (1997). Spatial characterization of water quality in Florida Bay and Whitewater Bay by principal component and cluster analyses: Zones of similar influence (ZSI). *Estuaries*, *20*, 743–758.

Cannizzaro, J. P., & Carder, K. L. (2006). Estimating chlorophyll a concentrations from remote-sensing reflectance in optically shallow waters. *Remote Sensing of Environment*, *101*, 13–24.

Cannizzaro, J. P., Hu, C., Carder, K. L., Kelble, C. R., Melo, N., Johns, E. M., et al. (in press). On the accuracy of SeaWiFS ocean color data products on the West Florida Shelf. *Journal of Coastal Research*.

Darecki, M., & Stramski, D. (2004). An evaluation of MODIS and SeaWiFS bio-optical algorithms in the Baltic Sea. *Remote Sensing of Environment*, *89*, 326–350.

Doron, M., Babin, M., Mangin, A., & Hembise, O. (2007). Estimation of light penetration, and horizontal and vertical visibility in oceanic and coastal waters from surface reflectance. *Journal of Geophysical Research*, *112*, C06003. http://dx.doi.org/10.1029/2006JC004007.

Duarte, C. M. (1991). Seagrass depth limits. *Aquatic Botany*, *40*, 363–377.

Gordon, H. R., & Ding, K. (1992). Self-shading of in-water optical instruments. *Limnology and Oceanography*, *37*, 491–500.

Gordon, H. R., & McCluney, W. R. (1975). Estimation of the depth of sunlight penetration in the sea for remote sensing. *Applied Optics*, *14*(2), 413–416.

Gregg, W. W., & Carder, K. L. (1990). A simple spectral solar irradiance model for cloudless martime atmospheres. *Limnology and Oceanography*, *35*, 1657–1675.

Gregg, W. W., & Casey, N. W. (2004). Global and regional evaluation of the SeaWiFS chlorophyll dataset. *Remote Sensing of Environment*, *93*, 463–479.

Hu, C., Lee, Z. P., Muller-Karger, F. E., & Carder, K. L. (2003a). Application of an optimization algorithm to satellite ocean color imagery: A case study in Southwest Florida coastal waters. In R. J. Frouin, Y. Yuan, & H. Kawamura (Eds.), *SPIE proceedings 4892. Ocean remote sensing and applications*. (pp. 70–79) Bellingham, WA: SPIE.

Hu, C., Muller-Karger, F. E., Biggs, D. C., Carder, K. L., Nababan, B., Nadeau, D., et al. (2003b). Comparison of ship and satellite bio-optical measurements on the continental margin of the NE Gulf of Mexico. *International Journal of Remote Sensing*, *24*, 2597–2612.

Hu, C., Muller-Karger, F. E., Vargo, G. A., Neely, M. B., & Johns, E. (2004a). Linkages between coastal runoff and the Florida Keys ecosystems: A study of a dark plume event. *Geophysical Research Letters*, *31*, L15307. http://dx.doi.org/10.1029/2004GL020382.

Hu, C., Nababan, B., Biggs, D. C., & Muller-Karger, F. E. (2004b). Variability of bio-optical properties at sampling stations and implications for remote sensing: A case study in the north-east Gulf of Mexico. *International Journal of Remote Sensing*, *25*, 2111–2120.

Kelble, C. R., & Boyer, J. N. (2007). Southern estuaries hypothesis cluster: Water quality. In Comprehensive Everglades Restoration Plan Assessment Team (Ed.), *Final 2007 System Status Report, 7-5-7.34*.

Kelble, C. R., Ortner, P. B., Hitchcock, G. L., & Boyer, J. N. (2005). Attenuation of photosynthetically available radiation (PAR) in Florida Bay: Potential for light limitation of primary producers. *Estuaries*, *28*, 560–571.

Kwiatkowska, E. J., Franz, B. A., Meister, G., McClain, C. R., & Xiong, X. (2008). Cross calibration of ocean-color bands from Moderate Resolution Imaging Spectroradiometer on Terra platform. *Applied Optics*, *47*, 6796–6810.

Lee, Z. P., Carder, K. L., Steward, R. G., Peacock, T. G., Davis, C. O., & Mueller, J. L. (1997). Remote-sensing reflectance and inherent optical properties of oceanic waters derived from above-water measurements. In S. G. Ackleson & R. Frouin (Eds.), *Proceedings of the Ocean Optics XIII Conference*, *Vol. 2963*. (pp. 1960–1966)Bellingham, WA: SPIE (Halifax, Nova Scotia).

Lee, Z., Carder, K. L., Mobley, C. D., Steward, R. G., & Patch, J. S. (1999). Hyperspectral remote sensing for shallow waters. 2. Deriving bottom depths and water properties by optimization. *Applied Optics*, *38*, 3831–3843.

Lee, Z. P., Carder, K. L., & Arnone, R. A. (2002). Deriving inherent optical properties from water color: A multiband quasi-analytical algorithm for optically deep waters. *Applied Optics*, *41*, 5755–5772. http://dx.doi.org/10.1364/AO.41.005755.

Lee, Z. P., Darecki, M., Carder, K., Davis, C., Stramski, D., & Rhea, W. (2005a). Diffuse attenuation coefficient of downwelling irradiance: An evaluation of remote sensing methods. *Journal of Geophysical Research*, *110*, C02017. http://dx.doi.org/10.1029/2004JC002573.

Lee, Z. P., Du, K., & Arnone, R. (2005b). A model for the diffuse attenuation coefficient of downwelling irradiance. *Journal of Geophysical Research*, *110*, C02016. http://dx.doi.org/10.1029/2004JC002275.

Lee, Z. P., & Hu, C. (2006). Global distribution of Case-1 waters: An analysis from SeaWiFS measurements. *Remote Sensing of Environment*, *101*, 270–276.

Lee, Z. P., Weidemann, A., Kindle, J., Arnone, R., Carder, K. L., & Davis, C. (2007). Euphotic zone depth: Its derivation and implication to ocean-color remote sensing. *Journal of Geophysical Research*, *112*, C03009. http://dx.doi.org/10.1029/2006JC003802.

Maritorena, S., Morel, A., & Gentili, B. (1994). Diffuse reflectance of oceanic shallow waters: Influence of water depth and bottom albedo. *Limnology and Oceanography*, *39*(7), 1689–1703.

Marrari, M., Hu, C., & Daly, K. (2006). Validation of SeaWiFS chlorophyll-a concentrations in the Southern Ocean: A revisit. *Remote Sensing of Environment*, *105*, 367–375.

McClain, C. R. (2009). A decade of satellite ocean color observations. *Annual Review of Marine Science*, *1*, 19–42.

McClain, C. R., Feldman, G. C., & Hooker, S. B. (2004). An overview of the SeaWiFS project and strategies for producing a climate research quality global ocean bio-optical time series. *Deep-Sea Research II*, *51*, 5–42.

McKee, D., Cunningham, A., & Dudek, A. (2007). Optical water type discrimination and tuning remote sensing band-ratio algorithms: Application to retrieval of chlorophyll and $K_d(490)$ in the Irish and Celtic Seas. *Estuarine, Coastal and Shelf Science*, *73*, 827–834.

Mélin, F., Zibordi, G., & Berthon, J. -F. (2007). Assessment of satellite ocean color products at a coastal site. *Remote Sensing of Environment*, *10*, 192–215.

Mobley, C. D. (1999). Estimation of the remote-sensing reflectance from above-surface measurements. *Applied Optics*, *38*(36), 7442–7445.

Morel, A. (1988). Optical modeling of the upper ocean in relation to its biogenous matter content (Case I waters). *Journal of Geophysical Research*, *93*, 10749–10768.

Morel, A. (1998). *Minimum requirements for an operational ocean-color sensor for the open ocean. IOCCG Report, Vol. 1*, Dartmouth, Nova Scotia: IOCCG Project Office (46 pp.).

Morel, A., & Gentili, B. (2004). Radiation transport within oceanic (case 1) water. *Journal of Geophysical Research*, *109*, C06008. http://dx.doi.org/10.1029/2003JC002259.

Morel, A., & Maritorena, S. (2001). Bio-optical properties of oceanic waters: A reappraisal. *Journal of Geophysical Research*, *106*, 7163–7180.

Morel, A. Y., & Prieur, L. (1977). Analysis of variations in ocean color. *Limnology and Oceanography*, *22*, 709–722.

Morel, A., Gentili, B., Claustre, H., Babin, M., Bricaud, A., Ras, J., et al. (2007a). Optical properties of the "clearest" natural waters. *Limnology and Oceanography*, *52*(1), 217–229.

Morel, A., Huot, Y., Gentili, B., Werdell, P. J., Hooker, S. B., & Franz, B. A. (2007b). Examining the consistency of products derived from various ocean color sensors in open ocean (Case 1) waters in the perspective of a multi-sensor approach. *Remote Sensing of Environment*, *111*, 69–88.

Mueller, J. L. (2000). SeaWiFS algorithm for the diffuse attenuation coefficient, $K_d(490)$, using water-leaving radiances at 490 and 555 nm. In S. B. Hooker (Ed.), *SeaWiFS postlaunch calibration and validation analyses, part 3, NASA Goddard Space Flight Center, Greeenbelt, MD* (pp. 24–27).

Mueller, J. L., & Trees, C. C. (1997). Revised SeaWiFS prelaunch algorithm for diffuse attenuation coefficient $K_d(490)$. *NASA Technical Memorandum, TM-104566*(41), 18–21.

Mueller, J. L., Morel, A., Frouin, R., Davis, C., Arnone, R., Carder, K., et al. (2003). *Ocean Optics protocols for satellite ocean color sensor validation, Revision 4, Volume III: Radiometric measurements and data analysis protocols.* NASA Tech. Memo. 2003–21621, National Aeronautics and Space Administration, Goddard Space Flight Center, Greenbelt, Maryland.

O'Reilly, J. E., Maritorena, S., Mitchell, B. G., Siegel, D. A., Carder, K. L., Garver, S. A., et al. (1998). Ocean color chlorophyll algorithms for SeaWiFS. *Journal of Geophysical Research*, *103*, 24937–24953.

Schaeffer, B. A., Sinclair, G. A., Lehrter, J. C., Murrell, M. C., Kurtz, J. C., Gould, R. W., et al. (2011). An analysis of diffuse light attenuation in the northern Gulf of Mexico hypoxic zone using the SeaWiFS satellite data record. *Remote Sensing of Environment*, *115*(12), 3748–3757.

Smith, R. C., & Baker, K. S. (1984). Analysis of ocean optical data. *Proceedings of SPIE Society of Optical Engineering*, *478*, 119–126.

Stramska, M., Stramski, D., Hapter, R., Kaczmarek, S., & Stón, J. (2003). Bio-optical relationships and ocean color algorithms for the north polar region of the Atlantic. *Journal of Geophysical Research*, *108*(C5), 3143. http://dx.doi.org/10.1029/2001JC001195.

Wang, M., Son, S., & Harding, W., Jr. (2009). Retrieval of diffuse attenuation coefficient in the Chesapeake Bay and turbid ocean regions for satellite ocean color applications. *Journal of Geophysical Research*, *114*, C10011. http://dx.doi.org/10.1029/2009JC005286.